

**Properties of a New Group of Cosmic Nuclei:
Results from the Alpha Magnetic Spectrometer on Sodium,
Aluminum, and Nitrogen**

- SUPPLEMENTAL MATERIAL -

(AMS Collaboration)

6 For references see the main text.

7 *Detector.*— AMS is a general purpose high energy particle physics detector in space. The
8 layout of the detector is shown in Fig. S1. The key elements are the permanent magnet, the
9 silicon tracker, four planes of time of flight (TOF) scintillation counters, the array of antico-
10 incidence counters (ACCs), a transition radiation detector (TRD), a ring imaging Čerenkov
11 detector (RICH), and an electromagnetic calorimeter (ECAL). The three-dimensional imag-
12 ing capability of the 17 radiation length ECAL allows for an accurate measurement of the
13 energy E and the shower shape of e^\pm . The AMS coordinate system is concentric with the
14 magnet. The x axis is parallel to the main component of the magnetic field and the z axis
15 points vertically with $z = 0$ at the center of the magnet. The (y - z) plane is the bending
16 plane. Above, below, and downward-going refer to the AMS coordinate system. The central
17 field of the magnet is 1.4 kG. Before flight, the field was measured in 120 000 locations to an
18 accuracy of better than 2 G. On orbit, the magnet temperature varies from -3 to $+20$ °C.
19 The field strength is corrected with a measured temperature dependence of $-0.09\%/\text{°C}$.
20 The tracker has nine layers, the first ($L1$) at the top of the detector, the second ($L2$) just
21 above the magnet, six ($L3$ to $L8$) within the bore of the magnet, and the last ($L9$) just
22 above the ECAL. $L2$ to $L8$ constitute the inner tracker. Each layer contains double-sided
23 silicon microstrip detectors, which independently measure the x and y coordinates. The
24 tracker accurately determines the trajectory of cosmic rays by multiple measurements of
25 the coordinates with a resolution in each layer of 6 μm for Na and 7 μm for Al nuclei in
26 the bending (y) direction. Together, the tracker and the magnet measure the rigidity R of
27 charged cosmic rays, with a maximum detectable rigidity of 3.3 TV for Na and 3.0 TV for
28 Al nuclei over the 3 m lever arm from $L1$ to $L9$.

29 Each layer of the tracker provides an independent measurement of the charge Z with a
30 resolution of $\sigma_Z/Z = 2.9\%$ for Na and Al nuclei. Overall, the inner tracker has a resolution
31 of $\sigma_Z/Z = 1.1\%$.

32 As seen from Fig. S1, two of the TOF planes are located above the magnet (upper TOF)
33 and two planes are below the magnet (lower TOF). The overall velocity ($\beta = v/c$) resolution
34 has been measured to be $\sigma(1/\beta) = 0.01$ for Na and Al nuclei. This discriminates between
35 upward- and downward-going particles. The pulse heights of the two upper planes are
36 combined to provide an independent measurement of the charge with an accuracy $\sigma_Z/Z = 2\%$.
37 The pulse heights from the two lower planes are combined to provide another independent
38 charge measurement with the same accuracy.

39 Na and Al nuclei traversing AMS were triggered as described in Ref. [24]. The trigger
40 efficiency has been measured to be $>95\%$ over the entire rigidity range for both Na and Al
41 nuclei.

42 Monte Carlo (MC) simulated events were produced using a dedicated program developed
43 by the collaboration based on the GEANT4-10.3 package [22]. The program simulates elec-
44 tromagnetic and hadronic [23] interactions of particles in the material of AMS and generates
45 detector responses. The digitization of the signals is simulated precisely according to the
46 measured characteristics of the electronics. The simulated events then undergo the same
47 reconstruction as used for the data.

48 *Event Selection.*— In the first 8.5 years AMS has collected 1.50×10^{11} cosmic ray events.
49 The collection time used in this analysis includes only those seconds during which the de-
50 tector was in normal operating conditions and, in addition, AMS was pointing within 40°
51 of the local zenith and the International Space Station was outside of the South Atlantic
52 Anomaly. Due to the geomagnetic field, this collection time increases with rigidity, reaching

53 1.98×10^8 s above 30 GV.

54 Na and Al nuclei events are required to be downward going and to have a reconstructed
55 track in the inner tracker which passes through $L1$. In the highest rigidity region, $R \geq$
56 1.2 TV, the track is also required to pass through $L9$. Track fitting quality criteria such as
57 a $\chi^2/\text{d.o.f.} < 10$ in the bending coordinate are applied.

58 Charge measurements on $L1$, the inner tracker, the upper TOF, the lower TOF, and, for
59 $R > 1.2$ TV, $L9$ are required to be compatible with charge $Z = 11$ for Na and $Z = 13$ for
60 Al.

61 The measured rigidity is required to be greater than a factor of 1.2 times the maximum
62 geomagnetic cutoff within the AMS field of view. The cutoff was calculated by backtrac-
63 ing [27] from the top of AMS out to 50 Earth's radii using the most recent International
64 Geomagnetic Reference Field model [28].

65 *Results of the study of cosmic ray propagation effects.*— To study the effect of cosmic ray
66 propagation on the Na/Si and Al/Si abundance ratio measurements at the source we used
67 the “slab” model studied in Ref. [33] as an example.

68 A fit of the $\Phi_{\text{Na}} = \Phi_{\text{Na}}^{\text{P}} + \Phi_{\text{Na}}^{\text{S}}$, with $\Phi_{\text{Na}}^{\text{P}} = k_{\text{Na}} \cdot e^{-\lambda_S(\tilde{\sigma}_{\text{Na}} - \tilde{\sigma}_{\text{Si}})} \times \Phi_{\text{Si}}$, where k_{Na} is the
69 Na/Si abundance ratio at the source and $e^{-\lambda_S(\tilde{\sigma}_{\text{Na}} - \tilde{\sigma}_{\text{Si}})}$ describes the propagation of primary
70 nuclei through the interstellar medium, see Eq. (3) from Ref. [33] with parameter $\Delta = 0$;
71 and $\Phi_{\text{Na}}^{\text{S}} = \kappa_{\text{Na}} \times \Phi_{\text{F}}$ was performed above 6 GV. The fit parameters are k_{Na} and κ_{Na} .
72 The definitions of $\lambda_S \propto \lambda$ and $\tilde{\sigma}$ are in Eqs.(4,5) from Ref. [33]. The λ parameter value
73 was fixed to 1 g/cm², see Table SA of Ref. [33]. The parameter Δ was set to zero by
74 assuming the same rigidity dependence of Na, Al, and Si fluxes at the source. The fit yields
75 $k_{\text{Na}} = 0.037 \pm 0.003$ and $\kappa_{\text{Na}} = 1.32 \pm 0.04$ with a $\chi^2/\text{d.o.f.} = 18/36$. Similarly, a fit of the
76 $\Phi_{\text{Al}} = \Phi_{\text{Al}}^{\text{P}} + \Phi_{\text{Al}}^{\text{S}}$, with $\Phi_{\text{Al}}^{\text{P}} = k_{\text{Al}} \cdot e^{-\lambda_S(\tilde{\sigma}_{\text{Al}} - \tilde{\sigma}_{\text{Si}})} \times \Phi_{\text{Si}}$ and $\Phi_{\text{Al}}^{\text{S}} = \kappa_{\text{Al}} \times \Phi_{\text{F}}$ was performed above
77 6 GV. The fit yields $k_{\text{Al}} = 0.104 \pm 0.004$ and $\kappa_{\text{Al}} = 1.00 \pm 0.04$ with a $\chi^2/\text{d.o.f.} = 24/36$.
78 The fit results are shown in Fig. S9.

79 Similar fits were done with “leaky box” model, see Eq. (6) from Ref. [33]. A fit of the
80 $\Phi_{\text{Na}} = \Phi_{\text{Na}}^{\text{P}} + \Phi_{\text{Na}}^{\text{S}}$, with $\Phi_{\text{Na}}^{\text{P}} = k_{\text{Na}} \cdot \frac{1+\lambda_S\tilde{\sigma}_{\text{Si}}}{1+\lambda_S\tilde{\sigma}_{\text{Na}}} \times \Phi_{\text{Si}}$, where k_{Na} is the Na/Si abundance ratio at
81 the source and $\frac{1+\lambda_S\tilde{\sigma}_{\text{Si}}}{1+\lambda_S\tilde{\sigma}_{\text{Na}}}$ describes the propagation of primary nuclei through the interstellar
82 medium, see Eq. (6) from Ref. [33] with parameter $\Delta = 0$ and the other parameters identical
83 to that used in the “slab” model; and $\Phi_{\text{Na}}^{\text{S}} = \kappa_{\text{Na}} \times \Phi_{\text{F}}$ was performed above 6 GV. The
84 parameter Δ was set to zero by assuming the same rigidity dependence of Na, Al, and Si
85 fluxes at the source. The fit yields $k_{\text{Na}} = 0.036 \pm 0.003$ and $\kappa_{\text{Na}} = 1.34 \pm 0.04$ with a
86 $\chi^2/\text{d.o.f.} = 19/36$. Similarly, a fit of the $\Phi_{\text{Al}} = \Phi_{\text{Al}}^{\text{P}} + \Phi_{\text{Al}}^{\text{S}}$, with $\Phi_{\text{Al}}^{\text{P}} = k_{\text{Al}} \cdot \frac{1+\lambda_S\tilde{\sigma}_{\text{Si}}}{1+\lambda_S\tilde{\sigma}_{\text{Al}}} \times \Phi_{\text{Si}}$
87 and $\Phi_{\text{Al}}^{\text{S}} = \kappa_{\text{Al}} \times \Phi_{\text{F}}$ was performed above 6 GV. The fit yields $k_{\text{Al}} = 0.103 \pm 0.004$ and
88 $\kappa_{\text{Al}} = 1.02 \pm 0.04$ with a $\chi^2/\text{d.o.f.} = 24/36$.

89 These results show that the propagation effects on the Na/Si and Al/Si abundance ratio
90 measurements at the source are negligible in the models. The similarity of $\tilde{\sigma}_{\text{Na}}$, $\tilde{\sigma}_{\text{Al}}$, and $\tilde{\sigma}_{\text{Si}}$
91 ensures other propagation models are expected to yield the same results.

TABLE SI: The Na flux Φ_{Na} as a function of rigidity at the top of AMS in units of $[\text{m}^2 \cdot \text{sr} \cdot \text{s} \cdot \text{GV}]^{-1}$ including errors due to statistics (stat.); contributions to the systematic error from the trigger and acceptance (acc.); the rigidity resolution function and unfolding (unf.); the absolute rigidity scale (scale); and the total systematic error (syst.). The contribution of individual sources to the systematic error are added in quadrature to arrive at the total systematic error.

Rigidity [GV]	Φ_{Na}	$\sigma_{\text{stat.}}$	$\sigma_{\text{acc.}}$	$\sigma_{\text{unf.}}$	σ_{scale}	$\sigma_{\text{syst.}}$
2.15 – 2.40	(5.339	0.058	0.228	0.202	0.026	0.306) $\times 10^{-2}$
2.40 – 2.67	(5.047	0.049	0.209	0.094	0.015	0.230) $\times 10^{-2}$
2.67 – 2.97	(4.616	0.041	0.187	0.052	0.008	0.195) $\times 10^{-2}$
2.97 – 3.29	(4.058	0.035	0.162	0.040	0.003	0.167) $\times 10^{-2}$
3.29 – 3.64	(3.623	0.029	0.143	0.033	0.001	0.147) $\times 10^{-2}$
3.64 – 4.02	(3.077	0.024	0.121	0.025	0.002	0.124) $\times 10^{-2}$
4.02 – 4.43	(2.629	0.020	0.103	0.020	0.002	0.105) $\times 10^{-2}$
4.43 – 4.88	(2.214	0.016	0.086	0.015	0.003	0.088) $\times 10^{-2}$
4.88 – 5.37	(1.815	0.013	0.071	0.011	0.003	0.072) $\times 10^{-2}$
5.37 – 5.90	(1.503	0.011	0.058	0.008	0.003	0.059) $\times 10^{-2}$
5.90 – 6.47	(1.218	0.009	0.047	0.006	0.003	0.048) $\times 10^{-2}$
6.47 – 7.09	(9.911	0.074	0.383	0.045	0.022	0.386) $\times 10^{-3}$
7.09 – 7.76	(8.045	0.060	0.310	0.033	0.019	0.313) $\times 10^{-3}$
7.76 – 8.48	(6.757	0.050	0.260	0.026	0.017	0.262) $\times 10^{-3}$
8.48 – 9.26	(5.398	0.041	0.207	0.019	0.015	0.209) $\times 10^{-3}$
9.26 – 10.1	(4.308	0.035	0.165	0.014	0.012	0.166) $\times 10^{-3}$
10.1 – 11.0	(3.459	0.030	0.132	0.011	0.010	0.133) $\times 10^{-3}$
11.0 – 12.0	(2.794	0.025	0.107	0.008	0.008	0.107) $\times 10^{-3}$
12.0 – 13.0	(2.337	0.022	0.089	0.007	0.007	0.090) $\times 10^{-3}$
13.0 – 14.1	(1.847	0.019	0.070	0.005	0.006	0.071) $\times 10^{-3}$
14.1 – 15.3	(1.508	0.016	0.057	0.004	0.005	0.058) $\times 10^{-3}$
15.3 – 16.6	(1.195	0.013	0.045	0.003	0.004	0.046) $\times 10^{-3}$
16.6 – 18.0	(9.646	0.112	0.367	0.027	0.033	0.369) $\times 10^{-4}$
18.0 – 19.5	(7.933	0.095	0.302	0.023	0.028	0.304) $\times 10^{-4}$
19.5 – 21.1	(6.420	0.080	0.244	0.019	0.023	0.246) $\times 10^{-4}$
21.1 – 22.8	(5.100	0.066	0.194	0.015	0.019	0.196) $\times 10^{-4}$
22.8 – 24.7	(4.183	0.054	0.159	0.013	0.016	0.161) $\times 10^{-4}$
24.7 – 26.7	(3.348	0.045	0.128	0.011	0.013	0.129) $\times 10^{-4}$
26.7 – 28.8	(2.696	0.038	0.103	0.009	0.010	0.104) $\times 10^{-4}$
28.8 – 33.5	(1.967	0.021	0.075	0.007	0.008	0.076) $\times 10^{-4}$
33.5 – 38.9	(1.269	0.015	0.049	0.005	0.005	0.049) $\times 10^{-4}$
38.9 – 45.1	(8.666	0.119	0.333	0.037	0.036	0.337) $\times 10^{-5}$
45.1 – 52.2	(5.595	0.089	0.216	0.026	0.025	0.219) $\times 10^{-5}$
52.2 – 60.3	(3.740	0.069	0.145	0.018	0.017	0.147) $\times 10^{-5}$
60.3 – 69.7	(2.439	0.051	0.095	0.013	0.012	0.096) $\times 10^{-5}$
69.7 – 80.5	(1.581	0.039	0.062	0.008	0.008	0.063) $\times 10^{-5}$
80.5 – 93.0	(1.049	0.029	0.041	0.006	0.006	0.042) $\times 10^{-5}$
93.0 – 108	(6.984	0.217	0.275	0.038	0.042	0.281) $\times 10^{-6}$

Table continued

TABLE SI – (*Continued*).

Rigidity [GV]	Φ_{Na}	$\sigma_{\text{stat.}}$	$\sigma_{\text{acc.}}$	$\sigma_{\text{unf.}}$	σ_{scale}	$\sigma_{\text{syst.}}$
108 – 125	(4.359	0.161	0.173	0.024	0.029	0.177) $\times 10^{-6}$
125 – 147	(2.837	0.114	0.113	0.016	0.021	0.116) $\times 10^{-6}$
147 – 175	(1.775	0.080	0.071	0.010	0.015	0.073) $\times 10^{-6}$
175 – 211	(9.972	0.527	0.402	0.063	0.098	0.419) $\times 10^{-7}$
211 – 259	(5.559	0.340	0.226	0.043	0.066	0.240) $\times 10^{-7}$
259 – 330	(2.974	0.205	0.123	0.032	0.045	0.134) $\times 10^{-7}$
330 – 441	(1.382	0.112	0.058	0.023	0.028	0.068) $\times 10^{-7}$
441 – 660	(4.716	0.465	0.204	0.134	0.146	0.284) $\times 10^{-8}$
660 – 1200	(1.235	0.152	0.058	0.069	0.070	0.114) $\times 10^{-8}$
1200 – 3000	(0.113	0.063	0.009	0.006	0.009	0.014) $\times 10^{-8}$

TABLE SII: The Al flux Φ_{Al} as a function of rigidity at the top of AMS in units of $[\text{m}^2 \cdot \text{sr} \cdot \text{s} \cdot \text{GV}]^{-1}$ including errors due to statistics (stat.); contributions to the systematic error from the trigger and acceptance (acc.); the rigidity resolution function and unfolding (unf.); the absolute rigidity scale (scale); and the total systematic error (syst.). The contribution of individual sources to the systematic error are added in quadrature to arrive at the total systematic error.

Rigidity [GV]	Φ_{Al}	$\sigma_{\text{stat.}}$	$\sigma_{\text{acc.}}$	$\sigma_{\text{unf.}}$	σ_{scale}	$\sigma_{\text{syst.}}$
2.15 – 2.40	(4.788	0.055	0.207	0.370	0.023	0.425) $\times 10^{-2}$
2.40 – 2.67	(4.858	0.048	0.202	0.160	0.015	0.258) $\times 10^{-2}$
2.67 – 2.97	(4.794	0.042	0.193	0.081	0.008	0.210) $\times 10^{-2}$
2.97 – 3.29	(4.490	0.037	0.177	0.061	0.003	0.187) $\times 10^{-2}$
3.29 – 3.64	(4.023	0.031	0.156	0.047	0.001	0.163) $\times 10^{-2}$
3.64 – 4.02	(3.545	0.026	0.136	0.035	0.002	0.140) $\times 10^{-2}$
4.02 – 4.43	(3.070	0.022	0.116	0.026	0.003	0.119) $\times 10^{-2}$
4.43 – 4.88	(2.518	0.018	0.095	0.018	0.003	0.097) $\times 10^{-2}$
4.88 – 5.37	(2.067	0.014	0.078	0.013	0.003	0.079) $\times 10^{-2}$
5.37 – 5.90	(1.710	0.012	0.064	0.009	0.003	0.065) $\times 10^{-2}$
5.90 – 6.47	(1.405	0.010	0.052	0.007	0.003	0.053) $\times 10^{-2}$
6.47 – 7.09	(1.127	0.008	0.042	0.005	0.003	0.042) $\times 10^{-2}$
7.09 – 7.76	(9.238	0.064	0.345	0.039	0.022	0.347) $\times 10^{-3}$
7.76 – 8.48	(7.559	0.053	0.282	0.030	0.019	0.284) $\times 10^{-3}$
8.48 – 9.26	(6.066	0.044	0.226	0.023	0.016	0.228) $\times 10^{-3}$
9.26 – 10.1	(5.040	0.037	0.188	0.019	0.014	0.189) $\times 10^{-3}$
10.1 – 11.0	(4.050	0.032	0.151	0.015	0.012	0.152) $\times 10^{-3}$
11.0 – 12.0	(3.320	0.027	0.124	0.012	0.010	0.125) $\times 10^{-3}$
12.0 – 13.0	(2.722	0.024	0.102	0.010	0.008	0.102) $\times 10^{-3}$
13.0 – 14.1	(2.186	0.020	0.082	0.008	0.007	0.082) $\times 10^{-3}$
14.1 – 15.3	(1.820	0.017	0.068	0.006	0.006	0.069) $\times 10^{-3}$
15.3 – 16.6	(1.470	0.015	0.055	0.005	0.005	0.055) $\times 10^{-3}$
16.6 – 18.0	(1.180	0.012	0.044	0.004	0.004	0.045) $\times 10^{-3}$
18.0 – 19.5	(9.534	0.105	0.357	0.033	0.033	0.360) $\times 10^{-4}$
19.5 – 21.1	(7.895	0.089	0.296	0.028	0.028	0.299) $\times 10^{-4}$
21.1 – 22.8	(6.596	0.075	0.248	0.023	0.024	0.250) $\times 10^{-4}$
22.8 – 24.7	(5.247	0.061	0.198	0.019	0.019	0.200) $\times 10^{-4}$
24.7 – 26.7	(4.220	0.051	0.160	0.015	0.016	0.161) $\times 10^{-4}$
26.7 – 28.8	(3.456	0.043	0.131	0.013	0.013	0.132) $\times 10^{-4}$
28.8 – 33.5	(2.562	0.024	0.098	0.010	0.010	0.099) $\times 10^{-4}$
33.5 – 38.9	(1.709	0.018	0.066	0.007	0.007	0.066) $\times 10^{-4}$
38.9 – 45.1	(1.129	0.014	0.043	0.005	0.005	0.044) $\times 10^{-4}$
45.1 – 52.2	(7.586	0.105	0.293	0.032	0.033	0.296) $\times 10^{-5}$
52.2 – 60.3	(5.063	0.080	0.196	0.022	0.023	0.199) $\times 10^{-5}$
60.3 – 69.7	(3.382	0.061	0.131	0.015	0.016	0.133) $\times 10^{-5}$
69.7 – 80.5	(2.306	0.047	0.090	0.011	0.012	0.091) $\times 10^{-5}$
80.5 – 93.0	(1.455	0.034	0.057	0.007	0.008	0.058) $\times 10^{-5}$
93.0 – 108	(9.431	0.253	0.371	0.047	0.054	0.378) $\times 10^{-6}$

Table continued

TABLE SII – (*Continued*).

Rigidity [GV]	Φ_{Al}	$\sigma_{\text{stat.}}$	$\sigma_{\text{acc.}}$	$\sigma_{\text{unf.}}$	σ_{scale}	$\sigma_{\text{syst.}}$
108 – 125	(6.648	0.199	0.262	0.034	0.041	0.268) $\times 10^{-6}$
125 – 147	(4.202	0.139	0.167	0.022	0.028	0.170) $\times 10^{-6}$
147 – 175	(2.613	0.097	0.104	0.015	0.019	0.107) $\times 10^{-6}$
175 – 211	(1.567	0.066	0.063	0.010	0.013	0.065) $\times 10^{-6}$
211 – 259	(8.801	0.430	0.357	0.064	0.088	0.373) $\times 10^{-7}$
259 – 330	(4.702	0.258	0.193	0.044	0.058	0.206) $\times 10^{-7}$
330 – 441	(2.177	0.141	0.091	0.028	0.035	0.101) $\times 10^{-7}$
441 – 660	(9.124	0.650	0.391	0.190	0.214	0.484) $\times 10^{-8}$
660 – 1200	(2.286	0.208	0.105	0.091	0.097	0.169) $\times 10^{-8}$
1200 – 3000	(0.413	0.122	0.028	0.012	0.024	0.039) $\times 10^{-8}$

TABLE SIII: The sodium to silicon flux ratio $\Phi_{\text{Na}}/\Phi_{\text{Si}}$ as a function of rigidity including errors due to statistics (stat.); contributions to the systematic error from the trigger, acceptance, and background (acc.); the rigidity resolution function and unfolding (unf.); the absolute rigidity scale (scale); and the total systematic error (syst.). The statistical errors are the sum in quadrature of the ratios of sodium and silicon flux statistical errors to the corresponding flux values, multiplied by $\Phi_{\text{Na}}/\Phi_{\text{Si}}$. The systematic errors from the background subtraction, the trigger, and the event reconstruction and selection are likewise added in quadrature. The correlations in the systematic errors from the uncertainty in nuclear interaction cross sections, the unfolding and the absolute rigidity scale between the sodium and silicon fluxes have been taken into account in calculating the corresponding systematic errors of $\Phi_{\text{Na}}/\Phi_{\text{Si}}$. The contribution of individual sources to the systematic error are added in quadrature to arrive at the total systematic uncertainty.

Rigidity [GV]	$\Phi_{\text{Na}}/\Phi_{\text{Si}}$	$\sigma_{\text{stat.}}$	$\sigma_{\text{acc.}}$	$\sigma_{\text{unf.}}$	σ_{scale}	$\sigma_{\text{syst.}}$
2.15 – 2.40	0.2438	0.0029	0.0087	0.0105	0.0001	0.0137
2.40 – 2.67	0.2466	0.0027	0.0087	0.0052	0.0001	0.0101
2.67 – 2.97	0.2463	0.0025	0.0086	0.0030	0.0000	0.0091
2.97 – 3.29	0.2412	0.0023	0.0085	0.0025	0.0000	0.0088
3.29 – 3.64	0.2419	0.0022	0.0085	0.0022	0.0000	0.0088
3.64 – 4.02	0.2362	0.0021	0.0083	0.0019	0.0000	0.0085
4.02 – 4.43	0.2345	0.0020	0.0082	0.0017	0.0000	0.0084
4.43 – 4.88	0.2287	0.0019	0.0081	0.0015	0.0000	0.0082
4.88 – 5.37	0.2228	0.0018	0.0079	0.0013	0.0000	0.0080
5.37 – 5.90	0.2192	0.0018	0.0077	0.0012	0.0000	0.0078
5.90 – 6.47	0.2104	0.0017	0.0074	0.0010	0.0000	0.0075
6.47 – 7.09	0.2049	0.0017	0.0072	0.0009	0.0000	0.0073
7.09 – 7.76	0.1987	0.0016	0.0070	0.0008	0.0000	0.0070
7.76 – 8.48	0.2038	0.0017	0.0072	0.0008	0.0000	0.0072
8.48 – 9.26	0.1947	0.0016	0.0068	0.0007	0.0000	0.0069
9.26 – 10.1	0.1886	0.0017	0.0066	0.0006	0.0000	0.0066
10.1 – 11.0	0.1836	0.0017	0.0064	0.0006	0.0000	0.0065
11.0 – 12.0	0.1812	0.0018	0.0063	0.0006	0.0000	0.0064
12.0 – 13.0	0.1838	0.0019	0.0064	0.0006	0.0000	0.0064
13.0 – 14.1	0.1748	0.0019	0.0061	0.0005	0.0000	0.0061
14.1 – 15.3	0.1743	0.0020	0.0061	0.0005	0.0000	0.0061
15.3 – 16.6	0.1675	0.0020	0.0058	0.0005	0.0000	0.0059
16.6 – 18.0	0.1659	0.0021	0.0058	0.0005	0.0000	0.0058
18.0 – 19.5	0.1660	0.0022	0.0058	0.0005	0.0000	0.0058
19.5 – 21.1	0.1623	0.0022	0.0057	0.0005	0.0000	0.0057
21.1 – 22.8	0.1582	0.0022	0.0055	0.0005	0.0000	0.0055
22.8 – 24.7	0.1578	0.0022	0.0055	0.0005	0.0000	0.0055
24.7 – 26.7	0.1536	0.0022	0.0054	0.0005	0.0000	0.0054
26.7 – 28.8	0.1488	0.0023	0.0052	0.0005	0.0001	0.0052
28.8 – 33.5	0.1450	0.0017	0.0051	0.0005	0.0001	0.0051
33.5 – 38.9	0.1369	0.0018	0.0048	0.0005	0.0001	0.0049
38.9 – 45.1	0.1381	0.0020	0.0049	0.0005	0.0001	0.0049

Table continued

TABLE SIII – (*Continued*).

Rigidity [GV]	$\Phi_{\text{Na}}/\Phi_{\text{Si}}$	$\sigma_{\text{stat.}}$	$\sigma_{\text{acc.}}$	$\sigma_{\text{unf.}}$	σ_{scale}	$\sigma_{\text{syst.}}$
45.1 – 52.2	0.1290	0.0022	0.0046	0.0005	0.0001	0.0047
52.2 – 60.3	0.1285	0.0025	0.0046	0.0006	0.0001	0.0047
60.3 – 69.7	0.1215	0.0027	0.0044	0.0006	0.0001	0.0045
69.7 – 80.5	0.1160	0.0030	0.0043	0.0006	0.0001	0.0043
80.5 – 93.0	0.1129	0.0033	0.0042	0.0006	0.0001	0.0042
93.0 – 108	0.1134	0.0037	0.0042	0.0006	0.0001	0.0043
108 – 125	0.1063	0.0041	0.0040	0.0005	0.0001	0.0040
125 – 147	0.1071	0.0045	0.0040	0.0006	0.0002	0.0041
147 – 175	0.1028	0.0049	0.0039	0.0006	0.0002	0.0040
175 – 211	0.0962	0.0053	0.0037	0.0006	0.0002	0.0038
211 – 259	0.0899	0.0058	0.0035	0.0006	0.0003	0.0036
259 – 330	0.0908	0.0065	0.0036	0.0009	0.0004	0.0037
330 – 441	0.0841	0.0071	0.0034	0.0012	0.0005	0.0037
441 – 660	0.0726	0.0074	0.0031	0.0018	0.0007	0.0036
660 – 1200	0.0712	0.0091	0.0033	0.0034	0.0012	0.0049
1200 – 3000	0.0487	0.0277	0.0039	0.0023	0.0013	0.0047

TABLE SIV: The aluminum to silicon flux ratio $\Phi_{\text{Al}}/\Phi_{\text{Si}}$ as a function of rigidity including errors due to statistics (stat.); contributions to the systematic error from the trigger, acceptance, and background (acc.); the rigidity resolution function and unfolding (unf.); the absolute rigidity scale (scale); and the total systematic error (syst.). The statistical errors are the sum in quadrature of the ratios of aluminum and silicon flux statistical errors to the corresponding flux values, multiplied by $\Phi_{\text{Al}}/\Phi_{\text{Si}}$. The systematic errors from the background subtraction, the trigger, and the event reconstruction and selection are likewise added in quadrature. The correlations in the systematic errors from the uncertainty in nuclear interaction cross sections, the unfolding and the absolute rigidity scale between the aluminum and silicon fluxes have been taken into account in calculating the corresponding systematic errors of $\Phi_{\text{Al}}/\Phi_{\text{Si}}$. The contribution of individual sources to the systematic error are added in quadrature to arrive at the total systematic uncertainty.

Rigidity [GV]	$\Phi_{\text{Al}}/\Phi_{\text{Si}}$	$\sigma_{\text{stat.}}$	$\sigma_{\text{acc.}}$	$\sigma_{\text{unf.}}$	σ_{scale}	$\sigma_{\text{syst.}}$
2.15 – 2.40	0.2186	0.0028	0.0077	0.0148	0.0001	0.0166
2.40 – 2.67	0.2374	0.0026	0.0081	0.0069	0.0001	0.0107
2.67 – 2.97	0.2557	0.0025	0.0086	0.0039	0.0000	0.0095
2.97 – 3.29	0.2669	0.0025	0.0089	0.0033	0.0000	0.0095
3.29 – 3.64	0.2686	0.0023	0.0089	0.0029	0.0000	0.0094
3.64 – 4.02	0.2721	0.0023	0.0090	0.0025	0.0000	0.0093
4.02 – 4.43	0.2738	0.0022	0.0090	0.0022	0.0000	0.0093
4.43 – 4.88	0.2600	0.0020	0.0086	0.0018	0.0000	0.0088
4.88 – 5.37	0.2538	0.0019	0.0084	0.0015	0.0000	0.0085
5.37 – 5.90	0.2495	0.0019	0.0082	0.0013	0.0000	0.0083
5.90 – 6.47	0.2425	0.0019	0.0080	0.0012	0.0000	0.0081
6.47 – 7.09	0.2330	0.0018	0.0077	0.0010	0.0000	0.0078
7.09 – 7.76	0.2281	0.0018	0.0076	0.0009	0.0000	0.0076
7.76 – 8.48	0.2280	0.0018	0.0076	0.0009	0.0000	0.0076
8.48 – 9.26	0.2189	0.0017	0.0073	0.0008	0.0000	0.0073
9.26 – 10.1	0.2206	0.0018	0.0073	0.0008	0.0000	0.0074
10.1 – 11.0	0.2149	0.0019	0.0072	0.0008	0.0000	0.0072
11.0 – 12.0	0.2154	0.0019	0.0072	0.0007	0.0000	0.0072
12.0 – 13.0	0.2140	0.0021	0.0071	0.0007	0.0000	0.0072
13.0 – 14.1	0.2069	0.0021	0.0069	0.0007	0.0000	0.0069
14.1 – 15.3	0.2103	0.0022	0.0070	0.0007	0.0000	0.0071
15.3 – 16.6	0.2061	0.0023	0.0069	0.0007	0.0000	0.0069
16.6 – 18.0	0.2029	0.0023	0.0068	0.0007	0.0000	0.0068
18.0 – 19.5	0.1995	0.0024	0.0067	0.0007	0.0000	0.0067
19.5 – 21.1	0.1996	0.0025	0.0067	0.0007	0.0000	0.0068
21.1 – 22.8	0.2046	0.0026	0.0069	0.0007	0.0000	0.0069
22.8 – 24.7	0.1980	0.0025	0.0067	0.0007	0.0000	0.0067
24.7 – 26.7	0.1937	0.0026	0.0066	0.0007	0.0000	0.0066
26.7 – 28.8	0.1907	0.0026	0.0065	0.0007	0.0000	0.0066
28.8 – 33.5	0.1889	0.0020	0.0065	0.0007	0.0000	0.0065
33.5 – 38.9	0.1844	0.0021	0.0064	0.0007	0.0001	0.0064
38.9 – 45.1	0.1800	0.0024	0.0063	0.0007	0.0001	0.0063

Table continued

TABLE SIV – (*Continued*).

Rigidity [GV]	$\Phi_{\text{Al}}/\Phi_{\text{Si}}$	$\sigma_{\text{stat.}}$	$\sigma_{\text{acc.}}$	$\sigma_{\text{unf.}}$	σ_{scale}	$\sigma_{\text{syst.}}$
45.1 – 52.2	0.1749	0.0026	0.0062	0.0007	0.0001	0.0062
52.2 – 60.3	0.1739	0.0030	0.0062	0.0007	0.0001	0.0062
60.3 – 69.7	0.1685	0.0033	0.0060	0.0007	0.0001	0.0061
69.7 – 80.5	0.1691	0.0037	0.0061	0.0007	0.0001	0.0061
80.5 – 93.0	0.1567	0.0040	0.0057	0.0007	0.0001	0.0057
93.0 – 108	0.1532	0.0044	0.0056	0.0007	0.0001	0.0056
108 – 125	0.1621	0.0052	0.0060	0.0008	0.0001	0.0060
125 – 147	0.1586	0.0057	0.0059	0.0008	0.0001	0.0059
147 – 175	0.1513	0.0060	0.0057	0.0008	0.0001	0.0057
175 – 211	0.1512	0.0069	0.0057	0.0009	0.0001	0.0058
211 – 259	0.1423	0.0074	0.0055	0.0010	0.0002	0.0055
259 – 330	0.1436	0.0085	0.0056	0.0012	0.0002	0.0057
330 – 441	0.1324	0.0091	0.0053	0.0016	0.0002	0.0055
441 – 660	0.1405	0.0107	0.0058	0.0026	0.0003	0.0064
660 – 1200	0.1317	0.0128	0.0058	0.0047	0.0003	0.0075
1200 – 3000	0.1774	0.0570	0.0126	0.0044	0.0002	0.0133

TABLE SV: The sodium to fluorine flux ratio $\Phi_{\text{Na}}/\Phi_{\text{F}}$ as a function of rigidity including errors due to statistics (stat.); contributions to the systematic error from the trigger, acceptance, and background (acc.); the rigidity resolution function and unfolding (unf.); the absolute rigidity scale (scale); and the total systematic error (syst.). The statistical errors are the sum in quadrature of the ratios of sodium and fluorine flux statistical errors to the corresponding flux values, multiplied by $\Phi_{\text{Na}}/\Phi_{\text{F}}$. The systematic errors from the background subtraction, the trigger, and the event reconstruction and selection are likewise added in quadrature. The correlations in the systematic errors from the uncertainty in nuclear interaction cross sections, the unfolding and the absolute rigidity scale between the sodium and fluorine fluxes have been taken into account in calculating the corresponding systematic errors of $\Phi_{\text{Na}}/\Phi_{\text{F}}$. The contribution of individual sources to the systematic error are added in quadrature to arrive at the total systematic uncertainty.

Rigidity [GV]	$\Phi_{\text{Na}}/\Phi_{\text{F}}$	$\sigma_{\text{stat.}}$	$\sigma_{\text{acc.}}$	$\sigma_{\text{unf.}}$	σ_{scale}	$\sigma_{\text{syst.}}$
2.15 – 2.40	1.8064	0.0321	0.0698	0.0594	0.0002	0.0916
2.40 – 2.67	1.8428	0.0296	0.0698	0.0304	0.0001	0.0762
2.67 – 2.97	1.7918	0.0263	0.0671	0.0197	0.0000	0.0699
2.97 – 3.29	1.7329	0.0243	0.0644	0.0164	0.0000	0.0665
3.29 – 3.64	1.7264	0.0225	0.0640	0.0145	0.0000	0.0656
3.64 – 4.02	1.6871	0.0217	0.0624	0.0126	0.0000	0.0637
4.02 – 4.43	1.7110	0.0217	0.0633	0.0114	0.0000	0.0643
4.43 – 4.88	1.6968	0.0205	0.0627	0.0102	0.0000	0.0636
4.88 – 5.37	1.6735	0.0196	0.0619	0.0090	0.0000	0.0625
5.37 – 5.90	1.6807	0.0198	0.0621	0.0082	0.0000	0.0627
5.90 – 6.47	1.6503	0.0196	0.0610	0.0073	0.0000	0.0614
6.47 – 7.09	1.6448	0.0196	0.0607	0.0066	0.0000	0.0611
7.09 – 7.76	1.6488	0.0198	0.0608	0.0061	0.0000	0.0611
7.76 – 8.48	1.7109	0.0207	0.0630	0.0058	0.0000	0.0633
8.48 – 9.26	1.6836	0.0209	0.0619	0.0054	0.0000	0.0621
9.26 – 10.1	1.6512	0.0214	0.0606	0.0050	0.0000	0.0608
10.1 – 11.0	1.6417	0.0225	0.0602	0.0048	0.0000	0.0603
11.0 – 12.0	1.6798	0.0241	0.0615	0.0048	0.0000	0.0617
12.0 – 13.0	1.7321	0.0270	0.0633	0.0049	0.0001	0.0635
13.0 – 14.1	1.6836	0.0275	0.0615	0.0048	0.0001	0.0617
14.1 – 15.3	1.6951	0.0289	0.0619	0.0049	0.0001	0.0621
15.3 – 16.6	1.6734	0.0301	0.0611	0.0049	0.0001	0.0613
16.6 – 18.0	1.6921	0.0320	0.0618	0.0051	0.0001	0.0620
18.0 – 19.5	1.7594	0.0348	0.0643	0.0054	0.0001	0.0645
19.5 – 21.1	1.7610	0.0361	0.0645	0.0056	0.0001	0.0647
21.1 – 22.8	1.7495	0.0372	0.0642	0.0058	0.0001	0.0645
22.8 – 24.7	1.7056	0.0359	0.0628	0.0058	0.0002	0.0631
24.7 – 26.7	1.7909	0.0401	0.0662	0.0064	0.0002	0.0665
26.7 – 28.8	1.7804	0.0416	0.0660	0.0066	0.0002	0.0664
28.8 – 33.5	1.8255	0.0326	0.0682	0.0072	0.0002	0.0686
33.5 – 38.9	1.7991	0.0363	0.0679	0.0076	0.0003	0.0683
38.9 – 45.1	1.8742	0.0431	0.0715	0.0085	0.0004	0.0720

Table continued

TABLE SV – (*Continued*).

Rigidity [GV]	$\Phi_{\text{Na}}/\Phi_{\text{F}}$	$\sigma_{\text{stat.}}$	$\sigma_{\text{acc.}}$	$\sigma_{\text{unf.}}$	σ_{scale}	$\sigma_{\text{syst.}}$
45.1 – 52.2	1.8716	0.0499	0.0722	0.0091	0.0005	0.0728
52.2 – 60.3	1.9454	0.0601	0.0760	0.0100	0.0007	0.0766
60.3 – 69.7	2.0321	0.0730	0.0803	0.0111	0.0008	0.0810
69.7 – 80.5	2.0347	0.0845	0.0813	0.0116	0.0009	0.0821
80.5 – 93.0	2.0261	0.0958	0.0819	0.0121	0.0009	0.0828
93.0 – 108	2.3389	0.1295	0.0956	0.0144	0.0010	0.0967
108 – 125	1.9570	0.1212	0.0809	0.0124	0.0009	0.0819
125 – 147	1.9741	0.1334	0.0827	0.0132	0.0009	0.0837
147 – 175	2.2858	0.1815	0.0972	0.0166	0.0009	0.0986
175 – 211	2.2556	0.2095	0.0975	0.0191	0.0006	0.0994
211 – 259	2.0581	0.2149	0.0907	0.0217	0.0002	0.0933
259 – 330	1.9852	0.2303	0.0896	0.0285	0.0006	0.0940
330 – 441	2.2566	0.3205	0.1051	0.0481	0.0023	0.1156
441 – 660	2.1260	0.3614	0.1044	0.0758	0.0058	0.1292
660 – 1200	2.1387	0.4553	0.1179	0.1491	0.0168	0.1908
1200 – 3000	3.0106	3.2507	0.3037	0.1895	0.0284	0.3591

TABLE SVI: The aluminum to fluorine flux ratio $\Phi_{\text{Al}}/\Phi_{\text{F}}$ as a function of rigidity including errors due to statistics (stat.); contributions to the systematic error from the trigger, acceptance, and background (acc.); the rigidity resolution function and unfolding (unf.); the absolute rigidity scale (scale); and the total systematic error (syst.). The statistical errors are the sum in quadrature of the ratios of aluminum and fluorine flux statistical errors to the corresponding flux values, multiplied by $\Phi_{\text{Al}}/\Phi_{\text{F}}$. The systematic errors from the background subtraction, the trigger, and the event reconstruction and selection are likewise added in quadrature. The correlations in the systematic errors from the uncertainty in nuclear interaction cross sections, the unfolding and the absolute rigidity scale between the aluminum and fluorine fluxes have been taken into account in calculating the corresponding systematic errors of $\Phi_{\text{Al}}/\Phi_{\text{F}}$. The contribution of individual sources to the systematic error are added in quadrature to arrive at the total systematic uncertainty.

Rigidity [GV]	$\Phi_{\text{Al}}/\Phi_{\text{F}}$	$\sigma_{\text{stat.}}$	$\sigma_{\text{acc.}}$	$\sigma_{\text{unf.}}$	σ_{scale}	$\sigma_{\text{syst.}}$
2.15 – 2.40	1.6199	0.0294	0.0623	0.1137	0.0001	0.1297
2.40 – 2.67	1.7738	0.0287	0.0662	0.0510	0.0000	0.0836
2.67 – 2.97	1.8607	0.0272	0.0679	0.0276	0.0000	0.0733
2.97 – 3.29	1.9172	0.0265	0.0688	0.0231	0.0001	0.0726
3.29 – 3.64	1.9171	0.0246	0.0680	0.0195	0.0001	0.0708
3.64 – 4.02	1.9436	0.0244	0.0684	0.0167	0.0001	0.0705
4.02 – 4.43	1.9981	0.0247	0.0700	0.0147	0.0000	0.0715
4.43 – 4.88	1.9292	0.0228	0.0674	0.0122	0.0000	0.0685
4.88 – 5.37	1.9060	0.0218	0.0665	0.0104	0.0000	0.0673
5.37 – 5.90	1.9130	0.0220	0.0667	0.0092	0.0000	0.0673
5.90 – 6.47	1.9028	0.0220	0.0663	0.0082	0.0000	0.0669
6.47 – 7.09	1.8703	0.0217	0.0653	0.0074	0.0000	0.0657
7.09 – 7.76	1.8931	0.0221	0.0661	0.0070	0.0000	0.0665
7.76 – 8.48	1.9139	0.0227	0.0669	0.0067	0.0000	0.0672
8.48 – 9.26	1.8922	0.0229	0.0662	0.0064	0.0001	0.0665
9.26 – 10.1	1.9315	0.0243	0.0676	0.0064	0.0001	0.0679
10.1 – 11.0	1.9223	0.0256	0.0674	0.0063	0.0001	0.0676
11.0 – 12.0	1.9966	0.0277	0.0700	0.0065	0.0001	0.0703
12.0 – 13.0	2.0170	0.0306	0.0708	0.0065	0.0001	0.0711
13.0 – 14.1	1.9929	0.0316	0.0700	0.0064	0.0002	0.0703
14.1 – 15.3	2.0458	0.0337	0.0719	0.0066	0.0002	0.0722
15.3 – 16.6	2.0589	0.0357	0.0725	0.0067	0.0002	0.0728
16.6 – 18.0	2.0692	0.0377	0.0730	0.0069	0.0003	0.0733
18.0 – 19.5	2.1143	0.0406	0.0748	0.0071	0.0003	0.0751
19.5 – 21.1	2.1656	0.0429	0.0768	0.0075	0.0004	0.0772
21.1 – 22.8	2.2628	0.0461	0.0806	0.0080	0.0004	0.0810
22.8 – 24.7	2.1395	0.0434	0.0767	0.0077	0.0005	0.0770
24.7 – 26.7	2.2575	0.0487	0.0814	0.0084	0.0005	0.0818
26.7 – 28.8	2.2822	0.0513	0.0828	0.0087	0.0006	0.0833
28.8 – 33.5	2.3780	0.0407	0.0872	0.0094	0.0007	0.0877
33.5 – 38.9	2.4221	0.0466	0.0901	0.0102	0.0008	0.0906
38.9 – 45.1	2.4424	0.0538	0.0919	0.0109	0.0009	0.0925

Table continued

TABLE SVI – (*Continued*).

Rigidity [GV]	$\Phi_{\text{Al}}/\Phi_{\text{F}}$	$\sigma_{\text{stat.}}$	$\sigma_{\text{acc.}}$	$\sigma_{\text{unf.}}$	σ_{scale}	$\sigma_{\text{syst.}}$
45.1 – 52.2	2.5375	0.0645	0.0965	0.0119	0.0011	0.0972
52.2 – 60.3	2.6333	0.0776	0.1013	0.0131	0.0013	0.1021
60.3 – 69.7	2.8178	0.0963	0.1096	0.0147	0.0016	0.1106
69.7 – 80.5	2.9675	0.1165	0.1167	0.0163	0.0020	0.1179
80.5 – 93.0	2.8109	0.1263	0.1118	0.0161	0.0022	0.1130
93.0 – 108	3.1583	0.1676	0.1271	0.0189	0.0028	0.1285
108 – 125	2.9849	0.1733	0.1215	0.0186	0.0031	0.1230
125 – 147	2.9241	0.1860	0.1206	0.0193	0.0035	0.1221
147 – 175	3.3651	0.2532	0.1408	0.0245	0.0048	0.1430
175 – 211	3.5447	0.3095	0.1508	0.0300	0.0061	0.1539
211 – 259	3.2581	0.3182	0.1413	0.0343	0.0070	0.1456
259 – 330	3.1392	0.3401	0.1394	0.0445	0.0087	0.1466
330 – 441	3.5559	0.4749	0.1629	0.0744	0.0130	0.1795
441 – 660	4.1136	0.6408	0.1985	0.1427	0.0203	0.2453
660 – 1200	3.9573	0.7758	0.2135	0.2678	0.0255	0.3435
1200 – 3000	10.9663	10.6683	1.0360	0.6623	0.1761	1.2422

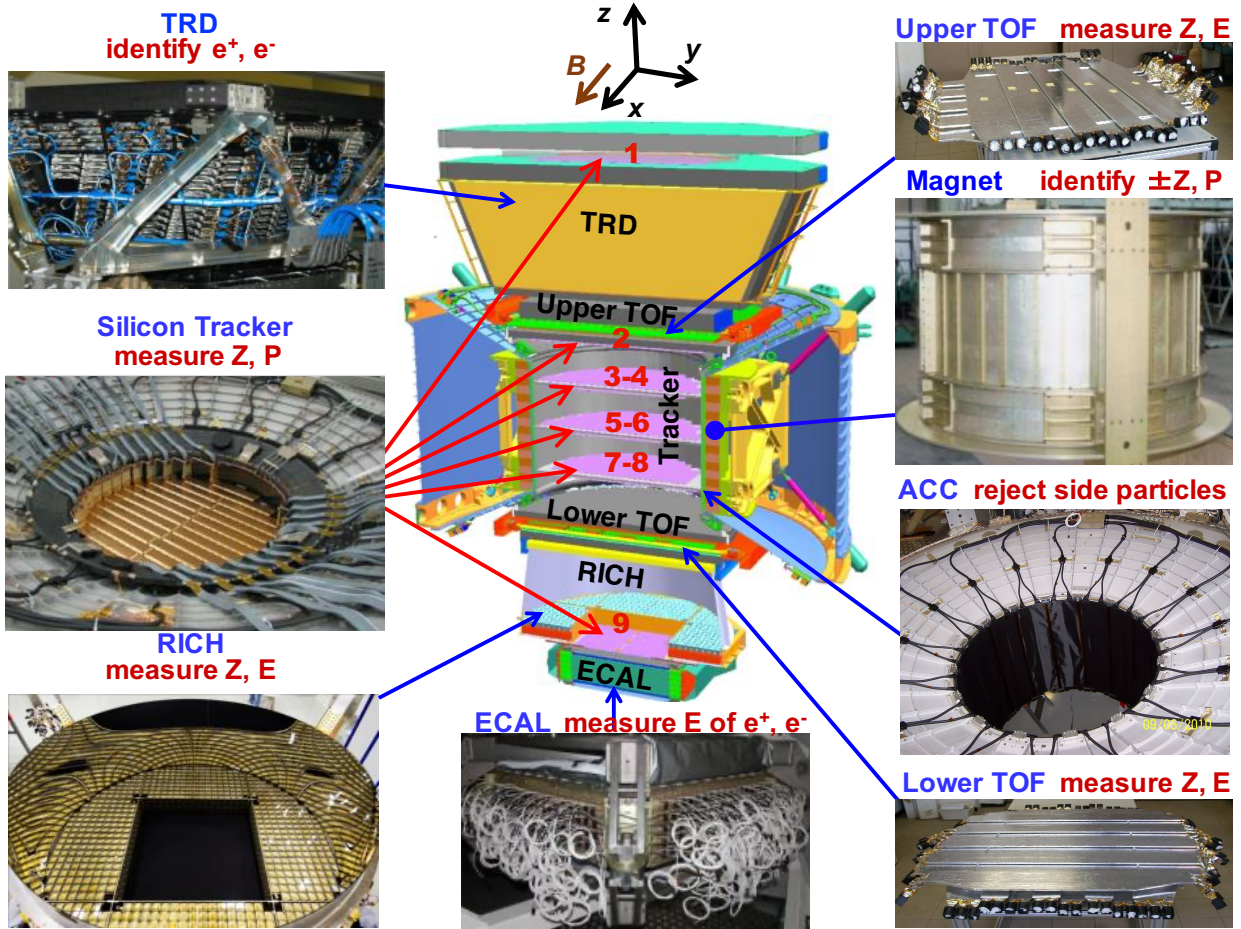


FIG. S1. The AMS detector showing the main elements and their functions. AMS is a TeV precision, multipurpose particle physics magnetic spectrometer in space. It identifies particles and nuclei by their charge Z , energy E and momentum P or rigidity ($R = P/Z$), which are measured independently by the Tracker, TOF, RICH and ECAL. The ACC counters, located in the magnet bore, are used to reject particles entering AMS from the side. The AMS coordinate system is also shown. The x axis is parallel to the main component of the magnetic field and the z axis is pointing vertically with $z = 0$ at the center of the magnet.

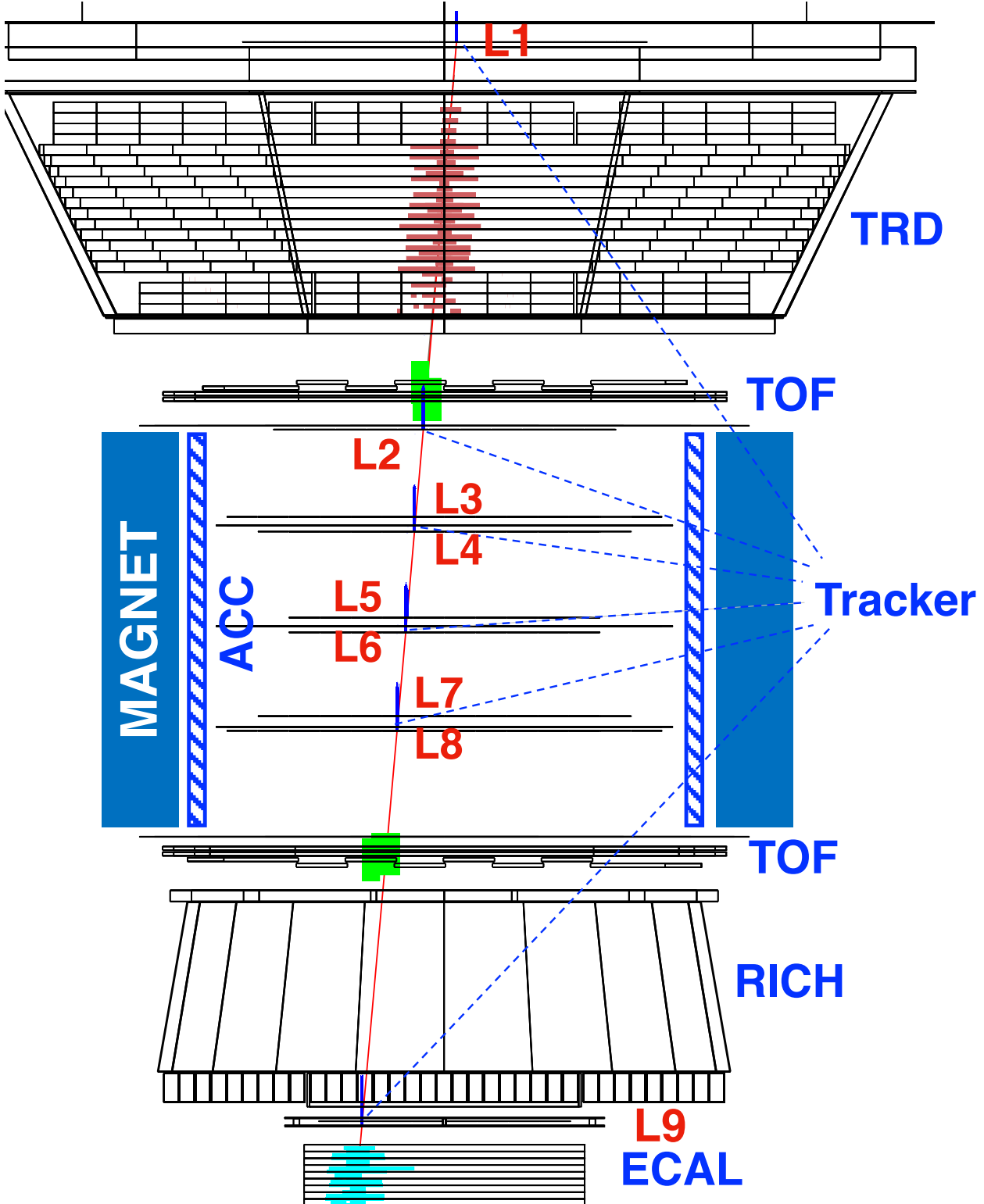


FIG. S2. A display of a sodium nucleus event in the bending plane. The red line indicates the reconstructed trajectory. The magenta spread in TRD shows the dE/dx measurements in different TRD layers, green areas in upper and lower TOF carry the information of the dE/dx as well as the coordinate and time measurements. The vertical blue lines in the tracker layers carry the information of coordinates and dE/dx or pulse heights. The light blue area in ECAL shows the shower development. This downward-going event is identified as a sodium nucleus ($Z=11$) with $R = 14$ GV.

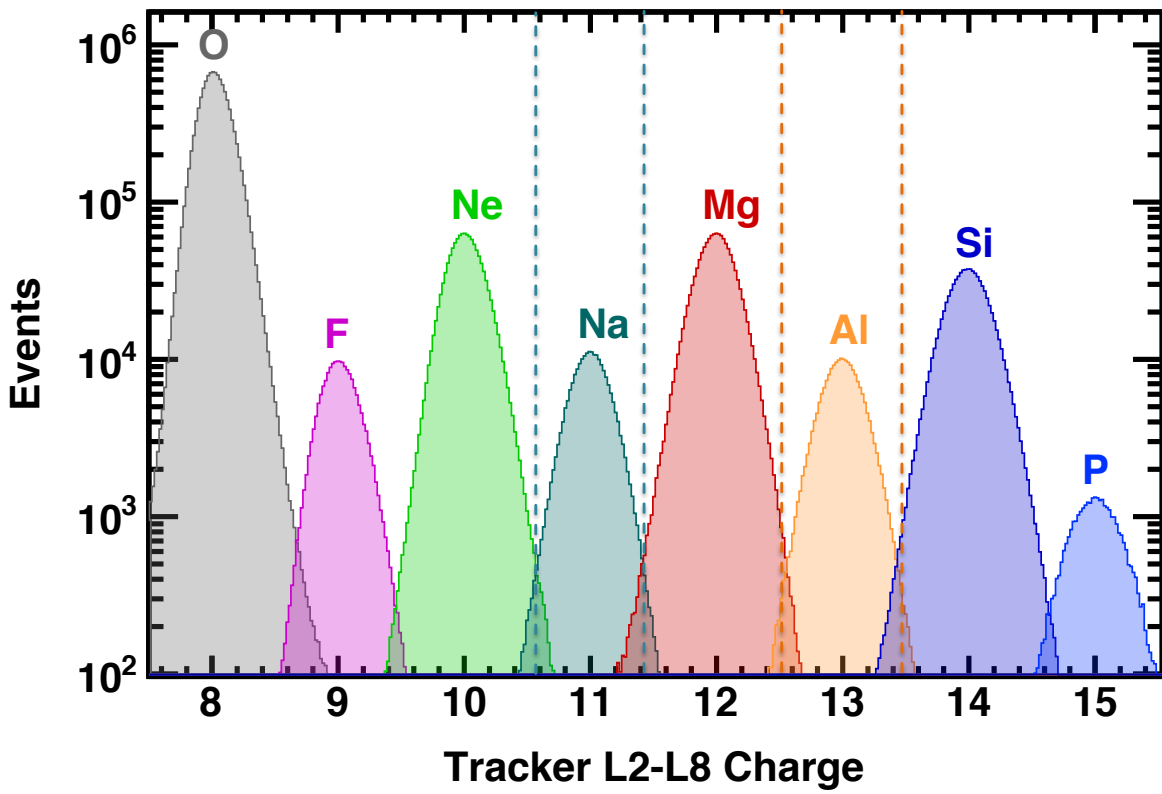


FIG. S3. Distribution of the charge measured with the inner tracker *L2-L8* for samples from $Z = 8$ to $Z = 15$ selected by the combined charge measured with *L1*, the upper TOF, and the lower TOF over the rigidities above 4 GV. The dashed vertical lines correspond to the charge selection in the inner tracker for sodium and aluminum.

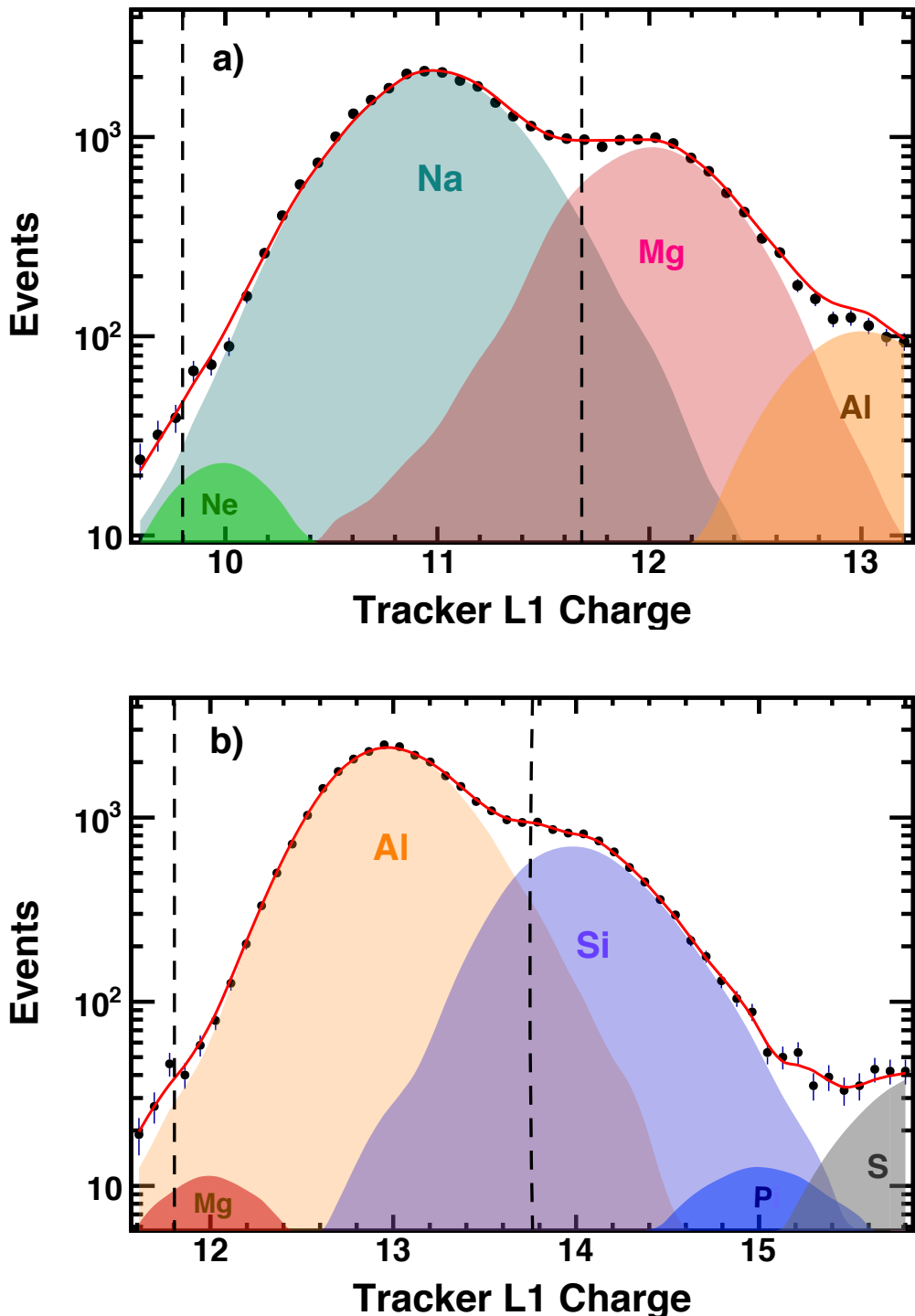


FIG. S4. Charge distributions measured by tracker *L1* for a) sodium events and b) aluminum events selected by the inner tracker *L2-L8* in the rigidity range between 18 and 22 GV (black dots). The solid red curves show the fits to the data of the sum of the Ne, Na, Mg, Al, Si, P, and S charge distribution templates. The templates are obtained from non-interacting samples at *L2* by using combined *L1*, upper TOF, *L3-L8*, and lower TOF charge selections. The charge selection applied on tracker *L1* is shown as vertical dashed lines.

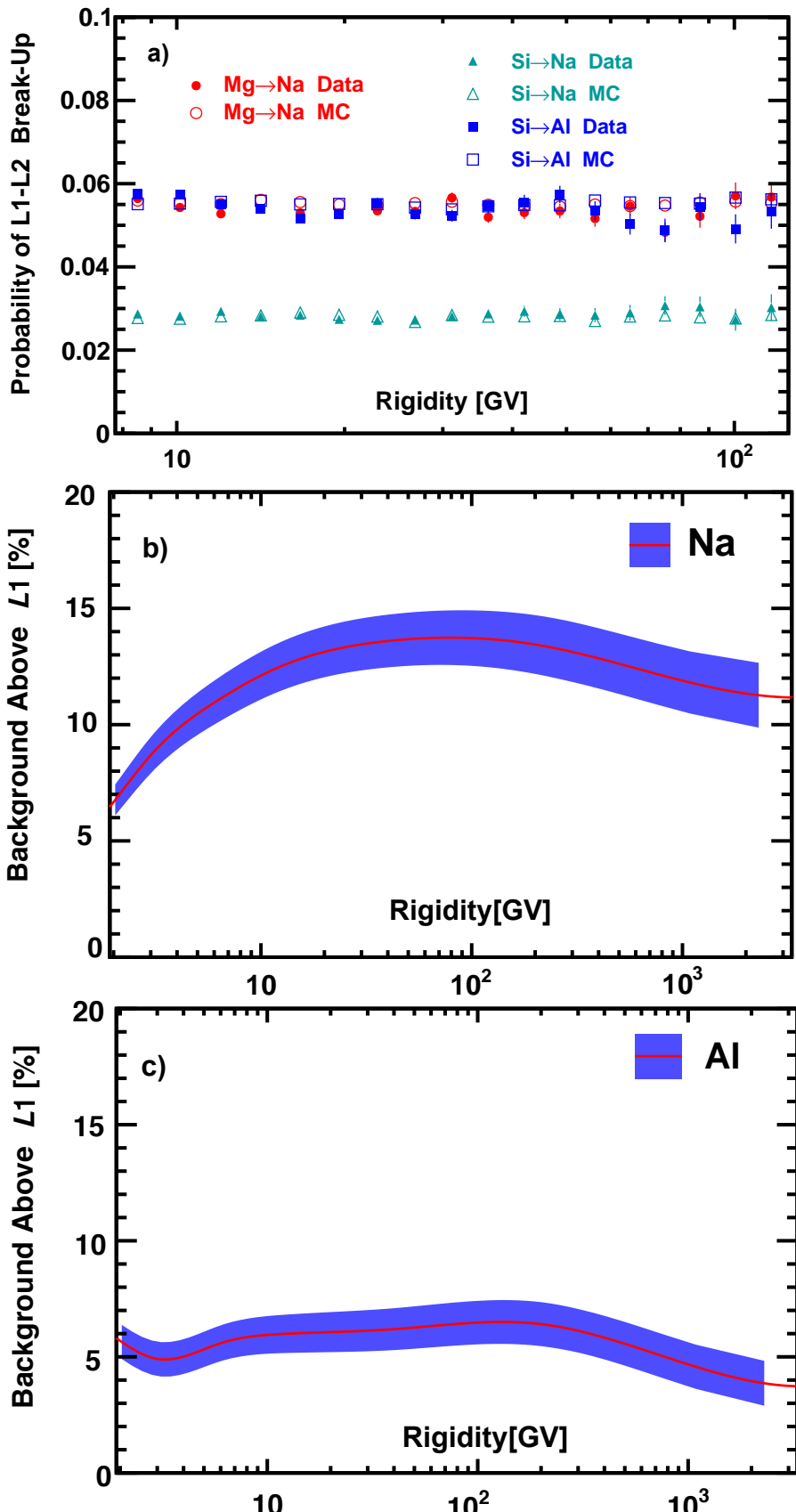


FIG. S5. a) Comparison of the measured data and simulated MC Mg \rightarrow Na+X, Si \rightarrow Na+X, and Si \rightarrow Al+X break-up probabilities between L_1 and L_2 . b) Na and c) Al background from heavier nuclei interactions above L_1 together with its uncertainty (blue shaded areas) as a function of rigidity. The amount of background as a function of rigidity is determined by nuclei interactions cross-sections, by the relative abundance of heavier nuclei to Na or Al, and by L_1 , upper TOF and lower TOF charge selection criteria, which were chosen to minimize the background uncertainty.

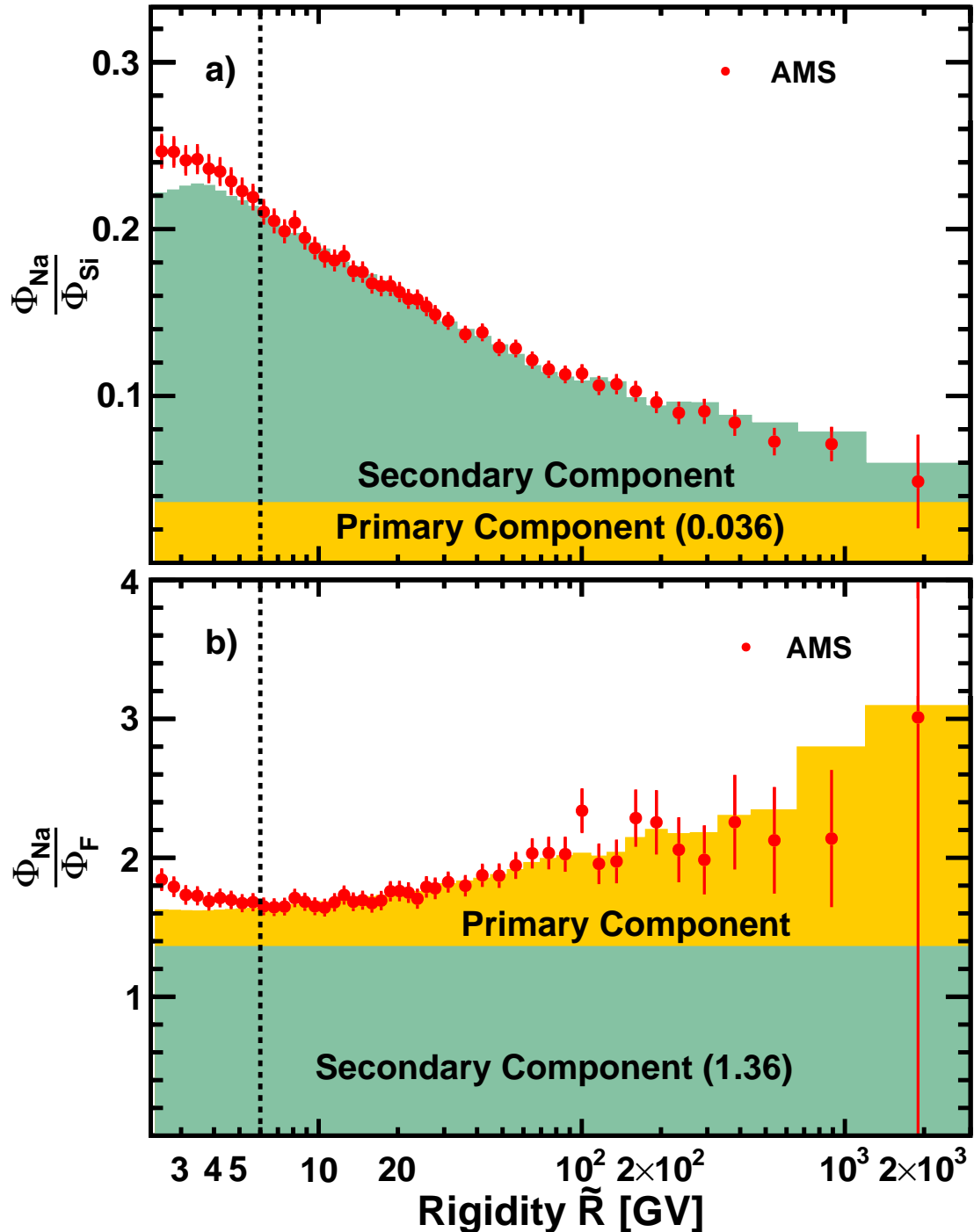


FIG. S6. a) $\Phi_{\text{Na}}/\Phi_{\text{Si}}$ as a function of rigidity. b) $\Phi_{\text{Na}}/\Phi_{\text{F}}$ as a function of rigidity. The contributions of the primary and secondary components are indicated by the shading (yellow and green, respectively). As seen, the contribution of secondary component in sodium flux decreases, and the contribution of primary component correspondingly increases with rigidity. The dashed vertical lines at 6 GV show the lower boundary of the fit range.

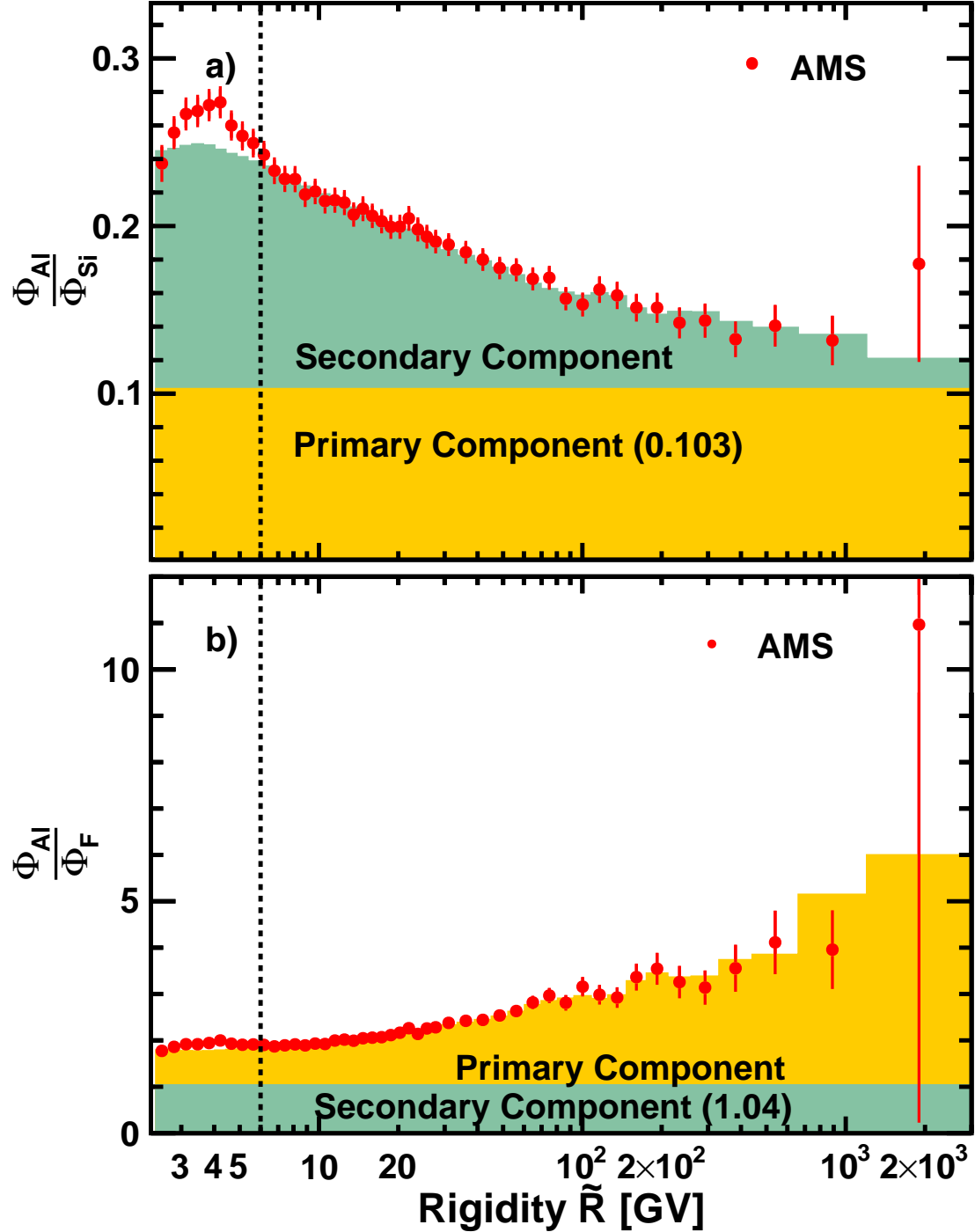


FIG. S7. a) $\Phi_{\text{Al}}/\Phi_{\text{Si}}$ as a function of rigidity. b) $\Phi_{\text{Al}}/\Phi_{\text{F}}$ as a function of rigidity. The contributions of the primary and secondary components are indicated by the shading (yellow and green, respectively). As seen, the contribution of secondary component in aluminum flux decreases, and the contribution of primary component correspondingly increases with rigidity. The dashed vertical lines at 6 GV show the lower boundary of the fit range.

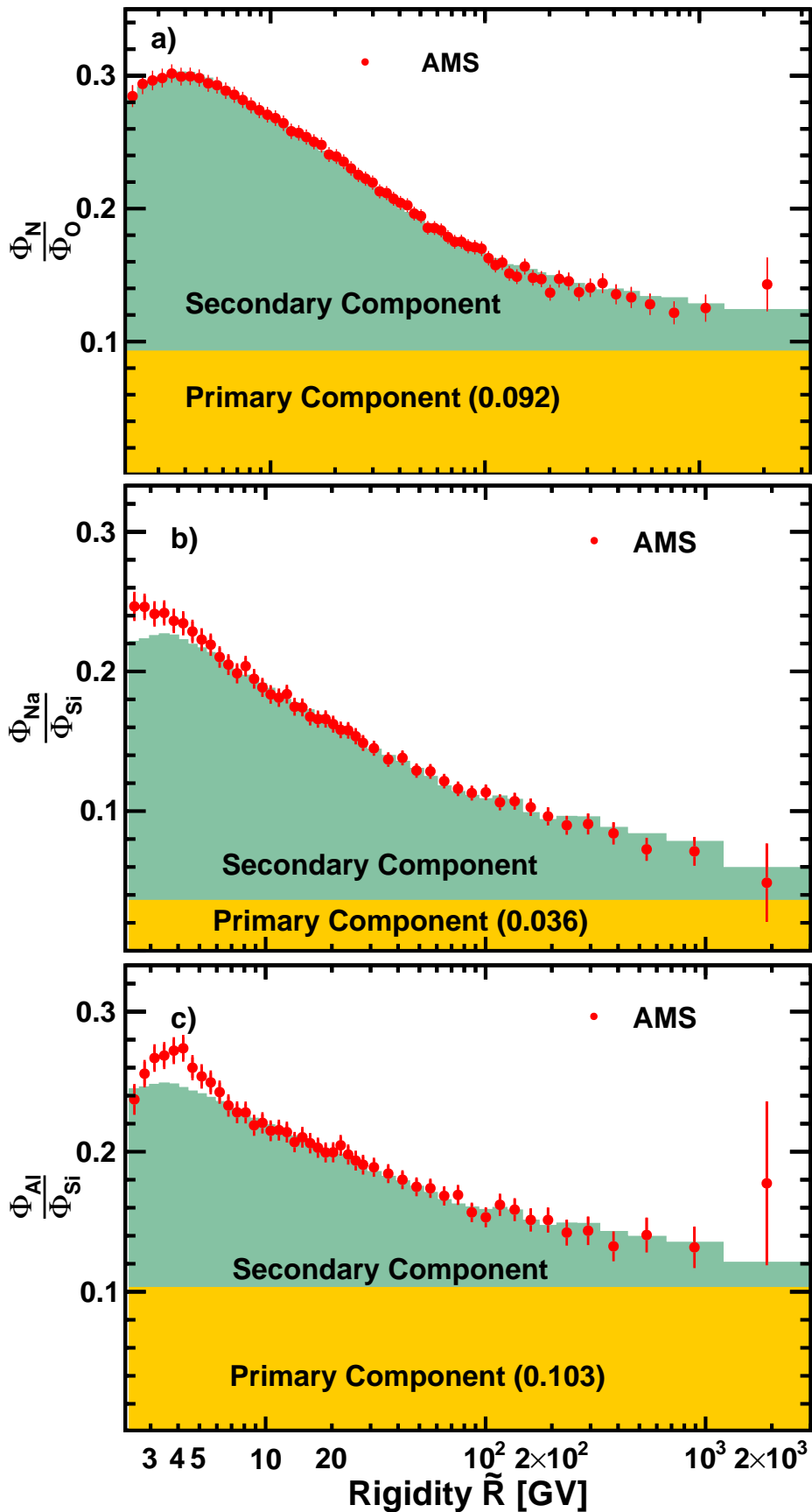


FIG. S8. a) Φ_N/Φ_O as a function of rigidity. b) Φ_{Na}/Φ_{Si} as a function of rigidity. c) Φ_{Al}/Φ_{Si} as a function of rigidity. The contributions of the primary and secondary components are indicated by the shading (yellow and green, respectively). As seen, the contribution of secondary component in all three fluxes decreases, and the contribution of primary component correspondingly increases with rigidity. Note that for nitrogen fit starts from 2.15 GV and for Na and Al from 6 GV.

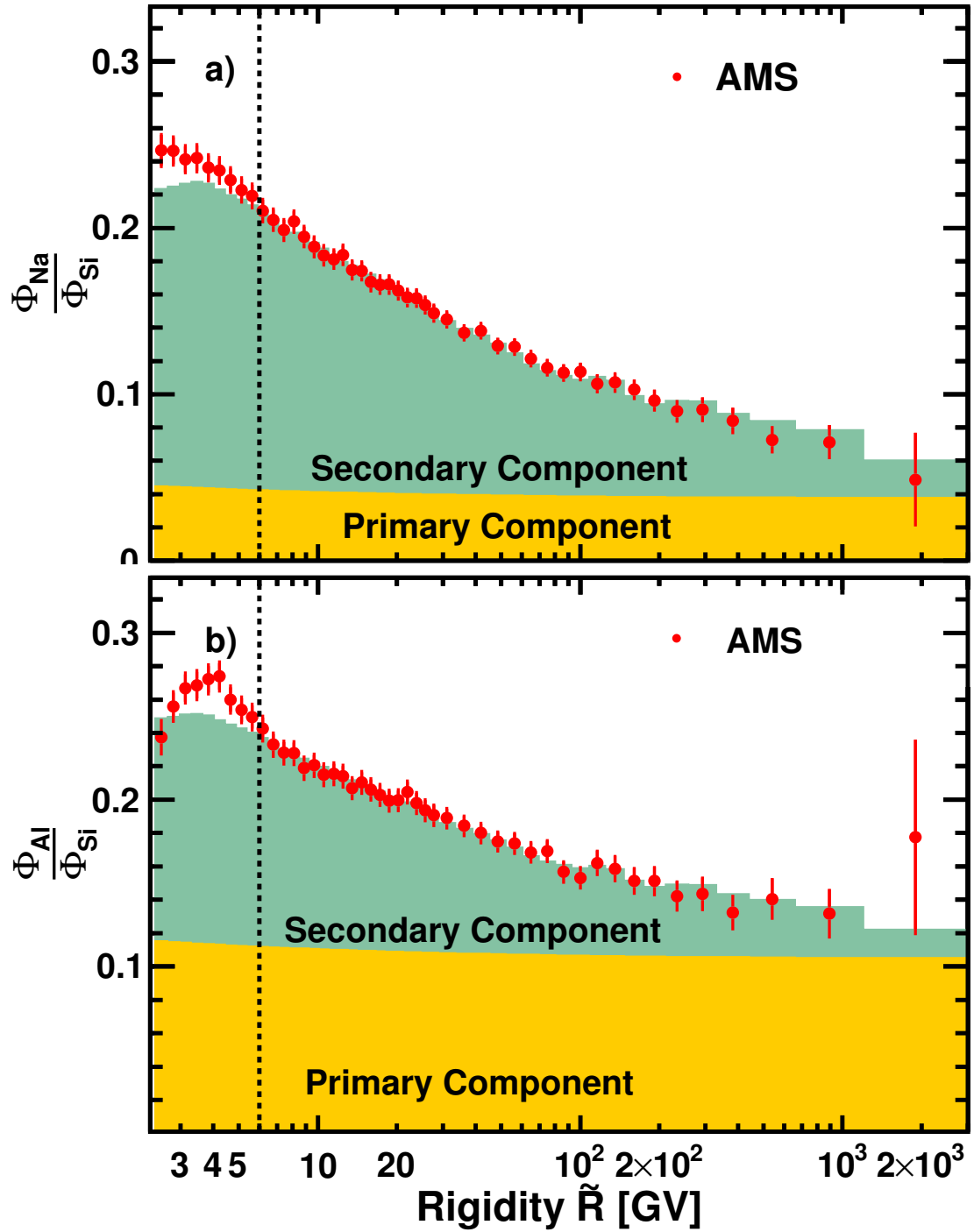


FIG. S9. a) $\Phi_{\text{Na}}/\Phi_{\text{Si}}$ as a function of rigidity. b) $\Phi_{\text{Al}}/\Phi_{\text{Si}}$ as a function of rigidity. The contributions of the primary and secondary components obtained by fits with the “slab” model are indicated by the shading (yellow and green, respectively). The dashed vertical lines at 6 GV show the lower boundary of the fit range.